HIGH ANGULAR RESOLUTION X-RAY OBSERVATIONS OF THE GALACTIC SUPERNOVA REMNANT G266.2−1.2 (RX J0852.0−4622)

T. G. Pannuti, J. W. Keohane
Spitzer Science Center, JPL/Caltech
MS 220-06, 1200 East California Blvd., Pasadena, CA 91125-0600, U.S.A.
TPANNUTI@IPAC.CALTECH.EDU, KEOHANE@IPAC.CALTECH.EDU
G. E. Allen, M. D. Filipović, M. Stupar, G. Goldstein
GEA@SPACE.MIT.EDU, M.FILIPOVIC@UWS.EDU.AU, MSTUPAR@ICS.MQ.EDU.AU, GREGGOLD@BLUEWIN.CH

Abstract

G266.2−1.2 (RX J0852.0−4622) is a member of the emerging class of Galactic supernova remnants (SNRs) which feature X-ray spectra dominated by non-thermal emission. This X-ray emission is believed to be synchrotron radiation produced by cosmic-ray electrons accelerated to TeV energies along the expanding shock fronts of SNRs. To explore this phenomenon of high energy X-ray emission from SNRs in more detail, we are conducting a broadband X-ray study of these sources using both new and archived observations. To illustrate this work, we present the results of our two observations made with *Chandra* (with a total effective exposure time of 73972 seconds) of the luminous northwestern rim of G266.2−1.2: this observation has revealed for the first time fine X-ray structure in this rim. A satisfactory fit to the spectrum of a sharply defined leading shock is derived using a power law model with a photon index $\Gamma = 2.41 \pm 0.06$. Alternatively, this spectrum can be fit with the SRCUT model which leads to an estimate of ≈ 40 TeV for the maximum energy of cosmic-ray electrons accelerated along this rim: however, additional radio observations of this rim are required to test more stringently the application of this model. Finally, we find that the spectra of regions located on and just interior to the rim may also be fit with a power law: a radial gradient in the values for the photon index may be explained as a localization of the acceleration of cosmic-ray particles to the shock region.

1 Introduction

Four Galactic supernova remnants (SNRs) are known to feature X-ray spectra dominated by non-thermal emission: SN1006 (Koyama et al., 1995; Winkler & Long, 1997; Allen et al., 2001; Dyer et al., 2001; Bamba et al., 2003; Long et al., 2003; Dyer et al., 2004), G28.6−0.1 (Bamba et al., 2001; Koyama et al., 2001; Ueno et al., 2003), G266.2−1.2 (Tsunemi et al., 2000; Slane et al., 2001) and G347.3−0.5 (Koyama et al., 1997; Slane et al., 1999; Pannuti et al., 2003; Uchiyama et al., 2003; Lazendic et al., 2004). It is currently believed that this non-thermal emission is synchrotron radiation produced by cosmic-ray electrons accelerated along the expanding shock front of these SNRs (Reynolds, 1998). This interpretation has been supported by qualitatively-consistent simple modeling of radio-to-X-ray synchrotron spectra (Reynolds & Keohane, 1999) as well as remarkably robust positional association between regions of hard X-ray emission and radio emission seen in images of these SNRs (Winkler & Long, 1997; Lazendic et al., 2004). A detailed study of this type of X-ray emission from SNRs holds great promise in resolving long-standing issues related to SNRs and cosmic-ray acceleration, including the maximum energy of cosmic-ray electrons accelerated by SNRs. This maximum energy may correspond to the well-known "knee" energy of the cosmic-ray spectrum ($\approx 10^{15}$ TeV): even higher energy cosmic-ray particles are believed to be accelerated by other classes of objects.

To develop a more thorough understanding of non-thermal X-ray emission from SNRs, we are currently

conducting an X-ray survey of these sources using both new and archived observations made by such observatories as *ROSAT*, *ASCA*, *RXTE* and *Chandra*. We are simultaneously modeling X-ray emission from these SNRs over an extremely broad energy range (from approximately 0.5 through 20 keV) as well as analyzing non-thermal emission from fine X-ray structure (on the order of arcseconds) in these sources as well. The primary goal of this research is to determine if SNRs can indeed accelerate cosmic-ray electrons to the maximum energies which approach the "knee" energy of the cosmic-ray spectrum. We illustrate this work in the present paper by describing our *Chandra* observation of the luminous northwestern rim of G266.2−1.2: this rim is known to feature an X-ray spectrum dominated by non-thermal emission.

2 G266.2−1.2 (RX J0852.0−4622)

G266.2−1.2 (RX J0852.0−4622) was discovered by Aschenbach (1998) during an X-ray survey conducted with *ROSAT* of the Vela SNR. The X-ray morphology of G266.2−1.2 (as seen in projection against Vela) is shell-like with three luminous rims: the spectra of each of these rims are known to be featureless and dominated by non-thermal emission (Slane et al., 2001). Since its discovery, there has been extensive debate about the true distance and age of G266.2−1.2: initially, an extremely short distance ($\sim$ 200 pc) and a very young age ($\sim$ 680 years) were argued based on a claimed detection of a γ-ray emission line associated with ^{44}Ti from this SNR (Iyudin et al., 1998) as well as an excess of calcium (presumed to be ^{44}Ca) in the X-ray spectra of the northwestern rim of G266.2−1.2 (Tsunemi et al., 2000). The detection of emission from these particular nuclei (thought to be closely associated with particularly young SNRs) formed the basis for arguments for classifying G266.2−1.2 as a very young SNR: this interpretation, combined with the large angular size of the SNR ($\sim 1\overset{\circ}{.}8$ in diameter), indicates that the SNR must be very nearby as well. However, Slane et al. (2001) argued against the presence of excess calcium in the X-ray spectrum of the northwestern rim of G266.2−1.2 and instead suggested that G266.2−1.2 is physically associated with the Vela Molecular Ridge, which is located at a distance of $\sim$ 1–2 kpc (Murphy, 1985). This result also suggests that G266.2−1.2 must be significantly older than previously claimed, with a dynamical age of at least 1000 years. The radio properties of this SNR have also been the subject of debate: while Combi et al. (1999) claimed to detect radio features that were coincident with the X-ray luminous rims of G266.2−1.2, Duncan & Green (2000) instead argued that these features were more likely associated with the Vela SNR instead of G266.2−1.2. The chief properties of G266.2−1.2 – namely an X-ray luminous shell-type SNR expanding into a low density ambient medium – are in common with the other SNRs which feature X-ray spectra dominated by non-thermal emission.

Table 1: *Chandra* observations of G266.2−1.2

ObsID	R.A. (J2000.0) (h m s)	Dec. (J2000.0) (° ′ ″)	Effective Exposure Time (seconds)
3816	08 49 09.39	−45 37 42.4	39452
4414	08 49 09.39	−45 37 42.4	34520

3 Observations and data reduction

Two pointed observations of the northwestern rim of G266.2−1.2 were conducted with *Chandra* between 2003 January 5-7: details of these two observations are summarized in Table 1 (the corresponding Sequence Number for these observations is 500325). During these observations, the telescope was pointed at a location along this rim and the total effective exposure time for the two observations was 73972 seconds. X-ray emission from this rim was detected using the Advanced CCD Imaging Spectrometer (ACIS) aboard *Chandra*: the ACIS is comprised of a 2×2 (ACIS-I) and a 1×6 (ACIS-S) array of CCDs. Six of these ten detectors (ACIS-I2, -S0, -S1, -S2, -S3, and -S4) were used for G266.2−1.2. Each 1024×1024 pixel CCD has a field of view of $8\overset{\prime}{.}4\times8\overset{\prime}{.}4$. The angular resolution of the *Chandra* mirrors and ACIS varies over the observed portion of the remnant from about $0\overset{\prime\prime}{.}5$ at the aim point to $7''$ for a region that is $10'$ off axis. The maximum on-axis effective area for the mirrors and ACIS-S3 is approximately 670 cm^2 at 1.5 keV: for energies between about 0.3 and 7.3 keV, the on-axis effective area is greater than 10% of this value. The fractional energy resolution (FWHM/E) between these energies ranges from about 0.4 to 0.03, respectively. The sensitive energy bands and energy resolutions of the other five CCDs used for the remnant are typically worse than the energy band and resolution of ACIS-S3.

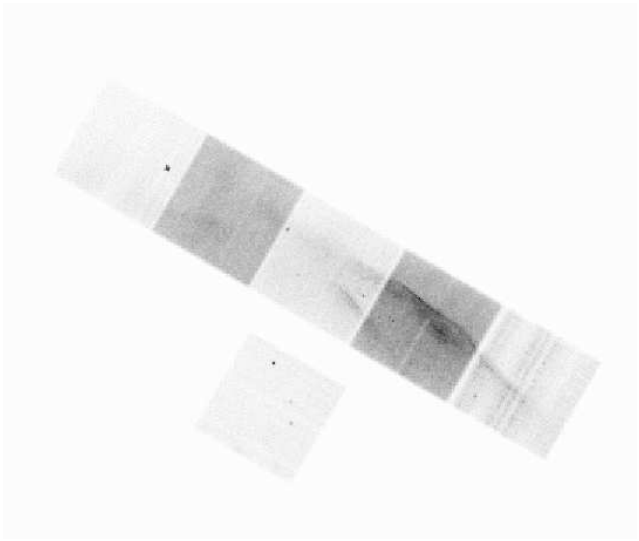

Figure 1: A *Chandra* image of the northwestern rim of G266.2−1.2. Notice the resolution of the rim into numerous fine X-ray structures: these fine structures have been revealed for the first time by our *Chandra* observations.

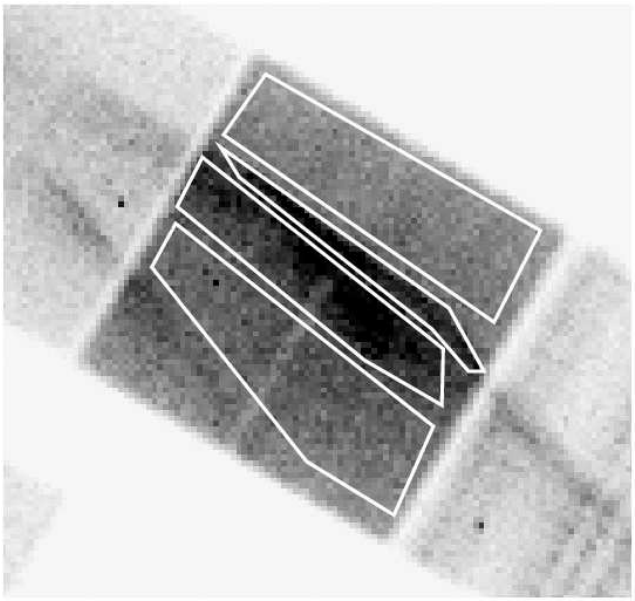

Figure 2: A portion of the northwestern rim of G266.2−1.2 as sampled by the ACIS-S3 chip aboard *Chandra*. We have extracted spectra from the four regions indicated here: the thin leading shock (Region #1), an X-ray bright region behind the shock (Region #2) and a fainter region (Region #3) farther behind Regions #1 and #2. We describe each region and analyze each spectra in Section 4.

The ACIS data were filtered to remove the events that (1) have GRADE = 1, 5, or 7, (2) have one or more of the STATUS bits set to one (except for events that only have one or more of the four cosmic-ray "afterglow" bits set), (3) occur on a bad pixel or column or (4) are part of a horizontal "streak" on ACIS-S4. The PHA spectra, ARFs and RMFs for each region were created using standard `CIAO` tools. The ARFs were adjusted for the effects of a build-up of absorbing material on the instruments. Our spectral analysis was conducted using the X-ray spectral analysis software package `XSPEC` (Version 11.3.0). In Fig. 1 we present an image of the northwestern rim of G266.2−1.2 as prepared from our observations. Our spectral analysis of particular X-ray features located along the rim (namely those features that were sampled by the S3 chip) is discussed in the next section.

4 Spectral analysis

Inspection of the X-ray image of the northwestern rim reveals fine structure in this rim which has been revealed for the first time through the high angular resolution capabilities of *Chandra*. To compare properties of different fine X-ray structures in this rim, we extracted spectra from three regions which were sampled by the ACIS-S3 chip during these two observations. We depict these three regions in Fig. 2: the first region encloses the very narrow shock front, the second region encloses a bright feature of X-ray emission which is just trailing behind the shock and the third region encloses diffuse X-ray emission which is located further behind the first two regions. For the remainder of this paper we will refer to these regions as Regions #1, #2 and #3, respectively. Diffuse X-ray emission from the Vela SNR is known to fill the entire field of view: this emission must be taken into account when analyzing the X-ray spectra of features associated with the northwestern rim of G266.2−1.2. For this reason, we also extracted a spectrum from an additional region located ahead of the prominent shock of the northwestern rim of G266.2−1.2: the position of this region is also indicated in Fig. 2.

We first consider the X-ray spectrum of the narrow shock front (Region #1): for this region we considered the energy range from 0.7 through 7.0 keV and fit the data using a simple power law model. For the intervening photoelectric absorption in this fit (as well as for every other fit described in the remainder of this paper), we applied the model WABS, which uses the Wisconsin cross-sections (Morrison & McCammon, 1983). We obtained an excellent fit (χ^2/degrees of freedom = 460.4/428 for a reduced χ^2 = 1.07) with

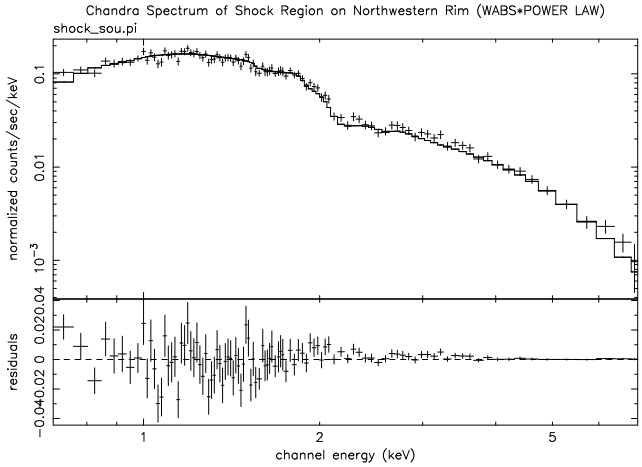

Figure 3: The spectrum of the region of the sharply-defined shock as fit with a power law model. See Section 4 for more details.

a column density N_H = 4.2±0.3×10^{21} cm^{-2}, a photon index Γ = 2.41±0.06 and a normalization at 1 keV of $8.11^{+0.56}_{-0.48}\times10^{-4}$ photons keV^{-1} cm^{-2} s^{-1} (all errors are at the 90% confidence level). We present the spectrum for this region (as fit by this model) in Fig. 3: we comment that our results are in broad agreement with those of Slane et al. (2001), who analyzed the X-ray spectrum of the entire northwestern rim as sampled by the Gas Imaging Spectrometer (GIS) aboard *ASCA* and also obtained a satisfactory fit to the spectrum with a power law model (N_H = 4.0±1.8×10^{21} cm^{-2} and Γ = 2.6±0.2). We attribute discrepancies between our derived spectral fits (particularly the differences in the photon indices) to the differences in the scale sizes considered in the two studies as well as the effects of confusing X-ray emission from Vela. We also point out that a thermal origin for the observed X-ray emission is ruled out by the absence of prominent lines in the spectrum presented in Fig. 3: we have also attempted to fit this emission using solely the thermal model MEKAL (Mewe et al., 1985, 1986; Liedahl et al., 1995) combined with WABS but we failed to obtain a statistically-acceptable fit (that is, a fit with a reduced $\chi^2 \approx 1$) with a thermal model.

To explore further the nature of the non-thermal X-ray emission from this shock region, we also fit the spectrum using the SRCUT model (Reynolds, 1998; Reynolds & Keohane, 1999) again combined with the WABS model. This model describes a synchrotron spectrum from a power law distribution (with an exponential cutoff) of electrons in a uniform magnetic field. The photon spectrum is itself a power law, rolling off more slowly than exponential in photon energies. The SRCUT model can be used to estimate the maximum energy of cosmic-ray electrons accelerated by G266.2−1.2: we assume that the relativistic electron energy spectrum $N_e(E)$ may be expressed as $N_e(E) = KE^{-\gamma}e^{-E/E_{\rm cutoff}}$, where K is a normalization constant derived from the observed flux density of the region of G266.2−1.2 at 1 GHz, γ is defined as 2α+1 (where α is the radio spectral index defined such that flux density $S_\nu \propto \nu^{-\alpha}$) and finally $E_{\rm cutoff}$ is the maximum energy of the accelerated cosmic-ray electrons. A crucial advantage of this model is that a resulting fit may be compared with two observable properties of G266.2−1.2, namely its flux density at 1 GHz and α. In addition, one of the fit parameters for this model is the cutoff frequency $\nu_{\rm cutoff}$ of the electron synchrotron spectrum, defined as the frequency at which the flux has dropped by a factor of 10 from a straight power law. This frequency may be expressed as

$$\nu_{\rm cutoff} \approx 1.66 \times 10^{16} \left(\frac{B_{\mu\rm G}}{10\ \mu\rm G}\right) \left(\frac{E_{\rm cutoff}}{10\ TeV}\right)^2 Hz, \quad (1)$$

where $B_{\mu\rm G}$ is the magnetic field of G266.2−1.2 in μG (we assume that the electrons are moving perpendicular to the magnetic field). By using the value for $\nu_{\rm cutoff}$ returned by SRCUT combined with the normalization factor K, the synchrotron spectrum of the shock-accelerated electrons can be adequately described. Moreover, an estimate for the maximum energy $E_{\rm cutoff}$ of the shock-accelerated cosmic-ray electrons may also be derived.

To constrain physically the fit derived to the spectrum using the SRCUT model, we first estimated the amount of radio flux at 1 GHz from this region. We calculated this based on the apparent angular size of G266.2−1.2 and a measured surface brightness at 1 GHz of 6.1±1.5×10^{-22} W m^{-2} Hz^{-1} sr^{-1} (Duncan & Green, 2000): based on these values, we calculated a flux density of 23 mJy for the shock region. We obtained a statistically acceptable fit (χ^2/degrees of freedom = 454.7/428 for a reduced χ^2 of 1.06) with the normalization frozen to 23 mJy, a column density N_H = 3.1±0.1×10^{21} cm^{-2} and a radio spectral index α = 0.50. We note that this value for the radio spectral index is consistent with the value of α = 0.40±0.15 that was estimated by Duncan & Green (2000). The value for the derived cutoff frequency in this fit is poorly con-

strained with a maximum value of $\nu_{\rm cutoff} = 2.42\times10^{17}$ Hz: if we assume a magnetic field strength of 10 μG (the strength of the magnetic field of G266.2−1.2 has yet to be measured), then from Equation 1 we estimate the maximum energy of cosmic-ray electrons accelerated along the northwestern rim of G266.2−1.2 to be $E_{\rm cutoff} \approx 40$ TeV. This energy is well short of the knee feature of the cosmic-ray spectrum: however, this result must be interpreted with some caution. For one reason, the radio properties of G266.2−1.2 as a whole and this rim in particular are poorly known: new radio observations conducted with high angular resolution which approach or correspond to the resolution of *Chandra* are required to test the applicability of the SRCUT model in a much more rigorous manner.

We now discuss our spectral fits to Regions #2 and #3: for both of these regions we considered flux over the energy range between 0.7 and 7.0 keV. Similar to our analysis of flux from Region #1, we found that a simple power law model returned statistically acceptable fits but the MEKAL model could not (again the WABS model was used in both cases for photoelectric absorption). For Region #2 our derived fit features a column density $N_H = 4.0\pm0.2\times10^{21}$ cm^{-2}, a photon index $\Gamma = 2.47\pm0.05$ and a normalization of $2.11\pm0.80\times10^{-3}$ photons keV^{-1} cm^{-2} s^{-1} at 1 keV (χ^2/degrees of freedom = 402.0/295 for a reduced χ^2 = 1.36), while for Region #3 our derived fit features a column density $N_H = 4.1\pm0.5\times10^{21}$ cm^{-2}, a photon index $\Gamma = 2.55\pm0.10$ and a normalization of $9.07\pm0.95\times10^{-4}$ photons keV^{-1} cm^{-2} s^{-1} at 1 keV (χ^2/degrees of freedom = 289.1/286 for a reduced χ^2 = 1.01). We summarize the results of our fits to the spectra extracted from all three regions in Table 2. It is very interesting to note that a gradient is seen in the values for the photon index for the three regions; that is, the photon index becomes steadily steeper as we consider regions more interior from the shock. Such a result indicates that cosmic-ray acceleration is taking place most dramatically at the location corresponding to the shock region (that is, Region #1): this result also illustrates an important application of the high angular resolution capabilities of *Chandra* in addressing the crucial issue of cosmic-ray acceleration by SNRs.

Table 2: Spectral fits using power law model

Region	Column Density N_H (10^{21} cm^{-2})	Photon Index Γ	Normalization (10^{-4} photons keV^{-1} cm^{-2} s^{-1} at 1 keV)
#1	4.2±0.3	2.41±0.06	$8.11^{+0.56}_{-0.48}$
#2	4.0±0.2	2.47±0.05	21.1±8.0
#3	4.1±0.5	2.55±0.10	9.07±0.95

5 Summary and future work

The results of this paper may be summarized as follows:

1) We have conducted two observations (with a total effective exposure time of 73972 seconds) with *Chandra* of the luminous northwestern rim of the Galactic SNR G266.2−1.2. This SNR is a member of the class of SNRs which feature X-ray spectra dominated by non-thermal emission: this emission is believed to have a synchrotron origin. To explore in detail the phenomenon of X-ray synchrotron emission from these SNRs, we are conducting a broadband X-ray study of the sources using both new and archived observations made with such observatories as *ROSAT*, *ASCA*, *RXTE* and *Chandra*.

2) We have analyzed X-ray spectra from three distinct regions along the northwestern rim of G266.2−1.2, ranging from a sharply defined shock located at the edge through two interior regions located on and just inside the rim. Satisfactory fits to the bright shock were derived separately using a power law model and the SRCUT model. Based on the parameters of the fit using the latter model we estimate the maximum energy of cosmic-ray electrons accelerated along the rim to be $\approx$ 40 TeV: this value is well short of the "knee" feature of the cosmic-ray spectrum. This result must be interpreted with caution until new more sensitive radio observations of this rim (with improved angular resolution) are conducted so that fits with the *SRCUT* model may be analyzed much more rigorously.

3) Satisfactory fits to the X-ray spectra from the two interior regions may also be derived using a simple power law model. We find that the value for the photon index becomes progressively steeper as we progress from the shock itself to regions located interior to the shock. This gradient indicates that cosmic-ray acceleration is taking place most efficiently at the region of the shock itself.

For future work we plan to analyze the spectral properties of other X-ray features associated with this rim

which were sampled by other ACIS chips during the *Chandra* observations. We will also incorporate into our analysis new complementary high angular resolution radio observations made of G266.2−1.2 with the Australia Telescope Compact Array (ATCA), the Molonglo Observatory Synthesis Telescope (MOST) and the Parkes radio telescope. This radio data will be included for modeling the properties of the synchrotron-emitting population of cosmic-ray electrons accelerated by this SNR over an extremely broad wavelength range (from radio through X-ray).

Acknowledgments

T.G.P. acknowledges useful discussions with Jeonghee Rho. T.G.P. also gratefully acknowledges support for this work from NASA Contract Number NAS8-39703.

References

Allen, G. E., Petre, R., Gotthelf, E. V. 2001, ApJ, 558, 739

Aschenbach, B. 1998, Nature, 396, 141

Aschenbach, B., Iyudin, A. F., Schönfelder, V. 1999, A&A, 350, 997

Bamba, A., Ueno, M., Koyama, K., Yamauchi, S. 2001, PASJ, 53, L21

Bamba, A., Yamazaki, R., Ueno, M., Koyama, K. 2003, ApJ, 589, 827

Combi, J. A., Romero, G. E., Benaglia, P. 1999, ApJ, 519, L177

Duncan, A. R., Green, D. A. 2000, A&A, 364, 732

Dyer, K. K., Reynolds, S. P., Borkowski, K. J., Allen, G. E., Petre, R. 2001, ApJ, 551, 439

Dyer, K. K., Reynolds, S. P., Borkowski, K. J. 2004, ApJ, 600, 752

Iyudin, A. F., et al. 1998, Nature, 396, 142

Koyama, K., et al. 1995, Nature, 378, 255

Koyama, K., et al. 1997, PASJ, 49, L7

Koyama, K., Ueno, M., Bamba, A., Ebisawa, K. 2001, Proceedings of the Symposium "New Visions of the X-ray Universe in the *XMM-Newton* and *Chandra* Era", Noordwijk, The Netherlands, 2001.

Lazendic, J. S., Slane, P. O., Gaensler, B. M., Reynolds, S. P., Plucinsky, P. P., Hughes, J. P. 2004, 602, 271

Liedahl, D. A., Osterheld, A. L., Goldstein, W. H. 1995, ApJ, 438, L115

Long, K. S., Reynolds, S. P., Raymond, J. C., Winkler, P. F., Dyer, K. K., Petre, R. 2003, ApJ, 586, 1162

Mewe, R., Gronenschild, E. H. B. M., van den Oord, G. H. J. 1985, A&AS, 62, 197

Mewe, R., Lemen, J. R., van den Oord, G. H. J. 1986, A&AS, 65, 511

Morrison, R., McCammon, D. 1983, ApJ, 270, 119

Murphy, D. C. 1985, Ph.D. Thesis, Massachusetts Institute of Technology

Pannuti, T. G., Allen, G. E., Houck, J. C., Sturner, S. J. 2003, ApJ, 593, 377

Reynolds, S. P. 1998, ApJ, 493, 375

Reynolds, S. P., Keohane, J. W. 1999, ApJ, 525, 368

Slane, P., Gaensler, B. M., Dame, T. M., Hughes, J. P., Plucinsky, P. P., Green, A. 1999, ApJ, 525, 357

Slane, P., et al. 2001, ApJ, 548, 814

Tsunemi, H., Miyata, E., Aschenbach, B., Hiraga, J., Akutsu, D. 2000, PASJ, 52, 887

Uchiyama, Y., Aharonian, F. A., Takahashi, T. 2003, A&A, 400, 567

Ueno, M., Bamba, A., Koyama, K., Ebisawa, K. 2003, ApJ, 588, 338

Winkler, P. F., Long, K. S. 1997, ApJ, 491, 829